Earth and Planetary Science Letters 497 (2018) 69–79

Contents lists available at ScienceDirect

Earth and Planetary Science Letters

www.elsevier.com/locate/epsl

# Crustal structure and deformation beneath eastern and northeastern Tibet revealed by P-wave receiver functions

Xu Wang [a,c], Ling Chen [a,c,d,*], Yinshuang Ai [b,c,d], Tao Xu [a,d], Mingming Jiang [b,d], Yuan Ling [a,c], Yifan Gao [a,c]

[a] State Key Laboratory of Lithospheric Evolution, Institute of Geology and Geophysics, Chinese Academy of Sciences, Beijing 100029, China
[b] Key Laboratory of Earth and Planetary Physics, Institute of Geology and Geophysics, Chinese Academy of Sciences, Beijing 100029, China
[c] University of Chinese Academy of Sciences, Beijing 100049, China
[d] CAS Center for Excellence in Tibetan Plateau Earth Sciences, Beijing 100101, China

ARTICLE INFO

*Article history:*
Received 31 January 2018
Received in revised form 1 June 2018
Accepted 6 June 2018
Available online xxxx
Editor: A. Yin

*Keywords:*
receiver function imaging
eastern Tibet
northeastern Tibet
crustal structure
crustal channel flow
wedging tectonics

ABSTRACT

The present-day Tibetan crust records the shallow response of the Cenozoic continental collision between the Indian and Eurasian plates. An analysis of the deep crustal structure beneath eastern and northeastern Tibet is of vital significance for studying the geodynamic processes of crustal thickening and expansion of the Tibetan Plateau. We herein provide detailed images of the crustal structure of eastern and northeastern Tibet and the adjacent Sichuan Basin using teleseismic P-wave receiver function (P-RF) data from a NW–SE-trending linear seismic array. Our P-RF imaging result reveals distinct structural features of the study region, including marked lateral variations in the depth to basement beneath the Songpan–Ganzi block and the Sichuan Basin, a seismically slow mid-lower crust beneath the Songpan–Ganzi block and a low-velocity anomaly just above the Moho around the easternmost Kunlun fault area, and obvious Moho offsets near the boundaries of tectonics blocks. These structural features may reflect various crustal responses within the continental interior to the India–Eurasia collision at the plate margin. The rigid crust of the Sichuan Basin might have wedged into the Tibetan crust in the Longmenshan area, which probably facilitated crustal thickening and enabled channelized mid-lower crustal flow in the Songpan–Ganzi block to the west. Being a pre-existing tectonic boundary, the Kunlun fault could have acted as a focus of heating and hot mantle upwelling associated with the deep processes of the Indian plate underthrusting and subduction, possibly resulting in localized weakening and modification of the lower crust around this fault area. The observed significant differences in the crustal structure of eastern and northeastern Tibet suggest that crustal shortening in this region may have been absorbed by not only vertical thickening in the interiors of the tectonic blocks but also complex local deformation along the boundary zones.



## 1. Introduction

The significant crustal thickening and high topography of Tibet were generated in response to the Indian–Eurasian continental collision that began during the Early Cenozoic (e.g., Yin and Harrison, 2000). However, to date, no consensus has been reached regarding the style of crustal deformation. Some models, including crustal channel flow and rigid block model, have been proposed to explain the tectonic deformation and high topography throughout the Tibeatan Plateau. The crustal channel flow model proposes that the lower crustal material beneath central Tibet is moving eastward, before being diverted towards the northeast and southeast around the Sichuan Basin (e.g., Royden et al., 1997); meanwhile, the rigid block model suggests that the India–Eurasia convergence is accommodated largely by the extrusion of material along strike-slip faults (Tapponnier et al., 2001). A recent study suggested that rigid block motion and crustal flow constitute two reconcilable modes of crustal deformation in eastern and southeastern Tibet, as both of these mechanisms significantly contribute to the eastward expansion of the Tibetan Plateau (Liu et al., 2014). In the eastern and northeastern areas of Tibet, however, it is unclear which mechanism is primarily responsible for the regional crustal deformation.

Detailed information of the crustal properties and structure in eastern and northeastern Tibet are crucial for reconstructing the processes of crustal deformation and regional orogenesis, which is however still lacking. In the eastern and northeastern Tibetan re-

* Corresponding author at: State Key Laboratory of Lithospheric Evolution, Institute of Geology and Geophysics, Chinese Academy of Sciences, Beijing 100029, China.
*E-mail address:* lchen@mail.iggcas.ac.cn (L. Chen).

https://doi.org/10.1016/j.epsl.2018.06.007
0012-821X/

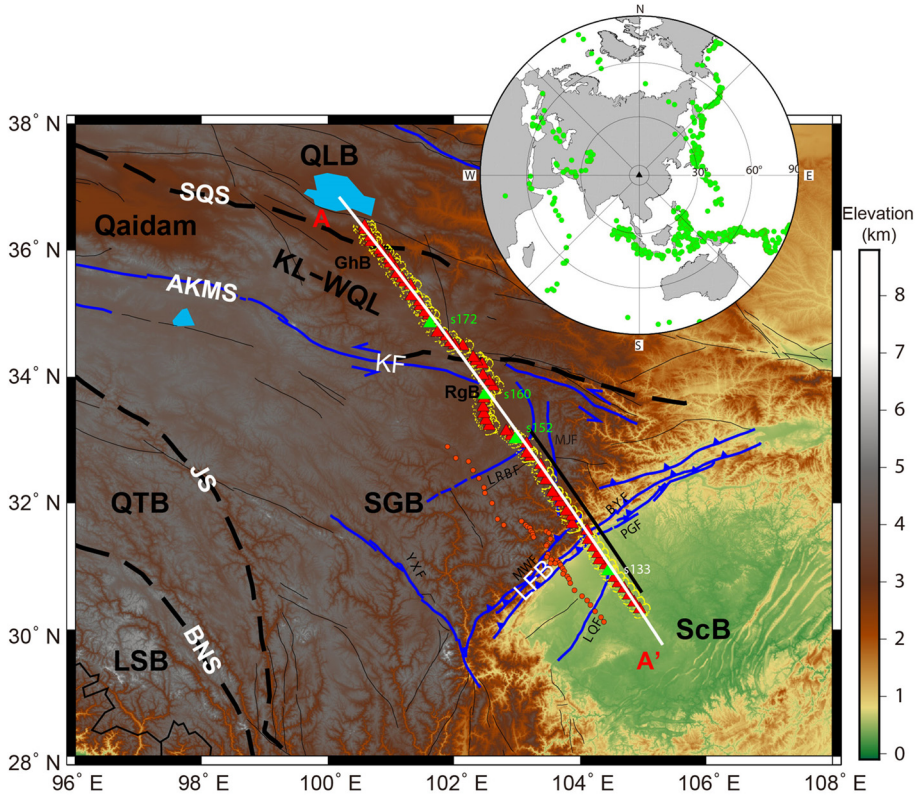


**Fig. 1.** Topographic map of eastern and northeastern Tibet and the Sichuan Basin, showing the locations of the broadband seismic stations (red and green triangles) and imaging profile (white straight line A–A′). Black dashed lines mark main sutures and blue solid lines represent main faults. Yellow dots show the piercing points at 50-km depth for *Ps* conversions. Red circles are the MT stations from Zhao et al. (2012). The black solid line delineates the tomographic imaging section from Wang et al. (2014). The inset map shows the distribution of teleseismic events used in this study. LSB: Lhasa block; QTB: Qiangtang block; SGB: Songpan–Ganzi block; Qaidam: Qaidam Basin; KL–WQL: Kunlun–West Qinling block; QLB: Qilian block; ScB: Sichuan Basin; GhB: Gonghe Basin; RgB: Ruoergai Basin; BNS: Bangong–Nujiang suture; JS: Jinsha river suture; AKMS: Anyimaqen–Kunlun–Muztagh suture; SQS: South Qilian suture; KF: Kunlun fault; LFB: Longmenshan fault belt; PGF: Pengxian–Guanxian fault; BYF: Beichuan–Yingxiu fault; MWF: Maoxian–Wenchuan fault; LRBF: Longriba fault; MJF: Minjiang fault; YXF: Yushu–Xianshuihe fault; LQF: Longquan fault. (For interpretation of the colors in the figure(s), the reader is referred to the web version of this article.)

gion that we are focusing on in this study, there are two major fault or fault systems (Fig. 1). One is the Kunlun fault within the Tibetan Plateau, which separates the Songpan–Ganzi block from the Kunlun–Qinling orogenic system to the north. The other is the Longmenshan (LMS) fault belt, the boundary zone between the Songpan–Ganzi block (Tibetan Plateau) in the west and the Yangtze Craton in the east. The LMS area, which is the site of the devastating Wenchuan earthquake, exhibits greater topographic relief than anywhere else in the marginal areas of the Tibetan Plateau. Numerous studies have been conducted across the LMS fault belt and several distinctive models have been proposed for the uplift of this area (see review by Yin, 2010), including upper crustal detachments (Hubbard and Shaw, 2009), mid-lower crustal channel flow (Royden et al., 1997) and wedging tectonics (Cai et al., 1996). The fundamental reason for the coexistence of these models is the uncertainties in the crustal structure of the eastern Songpan–Ganzi block, which is covered by a thick Triassic flysch complex (5–15 km; Nie et al., 1994). The nearly E–W-trending Kunlun fault represents a long transition from the flat, high-altitude central plateau in the south to the active tectonic domain characterized by ranges and intramontane basins in the north (Kirby et al., 2007). However, as indicated by the geophysical, geodetic and tectonic-geomorphological investigations (Kirby et al., 2007; Shen et al., 2005; Vergne et al., 2002; Wang et al., 2011; Xu et al., 2014; Zhang et al., 2011), the easternmost part of the Kunlun fault exhibits not only weaker variations in the crustal geometry but also reduced surface kinematics relative to the central-western part of the fault zone. Surface wave tomographic studies also observed a low-velocity anomaly with negative radial anisotropy ($V_{SH} < V_{SV}$) throughout the entire lithosphere and significant low-velocity characteristics with positive radial anisotropy in the asthenosphere right beneath the eastern section of the Kunlun fault (Li et al., 2016). A recent geomorphic analysis of longitudinal stream profiles in this area indicated a broad zone of rapid rock uplift (Kirby and Harkins, 2013). Moreover, in spite of the scarcity of heat flow sites, the measured heat fluxes near the easternmost part of the Kunlun fault and the Gonghe Basin are nearly twice as high as the average for the mainland of China (Jiang et al., 2016). The features, including seismically slow lithosphere–asthenosphere and high heat fluxes, support the scenario of an asthenosphere upwelling related to localized lithospheric delamination (Li et al., 2016). Such a process may locally induce the isostatic uplift of the surface, leading to local rapid rock uplift above (Kirby and Harkins, 2013; Li et al., 2016). Additionally, the result from a joint inversion of receiver function and Rayleigh wave dispersion data (Wu et al., 2017) suggests that the mid-lower crustal low-velocity zones (LVZs) beneath the Songpan–Ganzi block thin out around the transition zone between the Songpan–Ganzi block and the Kunlun–Qinling orogenic system. However, the results of ambient noise tomography conducted by Jiang et al. (2014) and magnetotelluric (MT) data from Pape et al. (2012) support the hypothesis that the crustal low-velocity and high-conductivity zones penetrate northward from the Songpan–Ganzi block into the Kunlun–Qinling orogen. Whether these LVZs are stopped by the Kunlun fault or have extruded to the north into the Kunlun–Qinling orogenic system remains obscure, as does the mechanism that contributes to the

presence of these LVZs, provided they exist, beneath the Kunlun–Qinling orogenic system.

Regarding the abovementioned scientific problems, in this study we investigated the crustal structure of the eastern and northeastern Tibetan region using teleseismic data from a NW–SE-trending linear seismic array across both the LMS fault belt and the easternmost part of the Kunlun fault. This array was deployed by the Institute of Geology and Geophysics, Chinese Academy of Sciences in 2010–2013 (details given in the Data and Methods section). Crustal structural images were constructed by applying a wave-equation based migration technique (Chen et al., 2005) to multiple seismic phases in the P-wave receiver functions (P-RFs) and average crustal $Vp/Vs$ ratios beneath individual stations obtained using the P-RF H–K stacking method (Zhu and Kanamori, 2000). Based on our new images and information from previous studies, we discuss the crustal structure and deformation associated with the interactions among different tectonic units, and construct a crustal model for the tectonic evolution of eastern and northeastern Tibet.

## 2. Geological setting

The Songpan–Ganzi block, which constitutes a main component of eastern Tibet, is an inverted triangular tectonic element separated from the Qaidam Basin and the Kunlun–West Qinling block by the Anyimaqen–Kunlun–Muztagh suture (AKMS) to the north, from the Sichuan Basin by the LMS fault belt to the east, and from the Qiangtang block by the Jinsha river suture to the west (Fig. 1). Thick Triassic strata, commonly named the Triassic flysch complex, are widely distributed throughout the Songpan–Ganzi block and the Kunlun–West Qinling area. Due to the thickness of the overlying flysch complex and the lack of deep-seated rocks at the surface, the nature of the basement beneath the Songpan–Ganzi block remains unclear. Triassic strata conformably overlie the Paleozoic shallow marine sequences of South China in the easternmost part of the block, suggesting that the basement is continental, at least in this area (Burchfiel et al., 1995). However, Sengör (1984) proposed that the Songpan–Ganzi block lacked a continental basement and that the flysch complex might be deposited directly atop the oceanic crust of a subduction zone. Many geophysical investigations revealed the presence of low-velocity zones or high-conductivity bodies in the mid-lower crust under the Songpan–Ganzi block (Jiang et al., 2014; Zhao et al., 2012), thereby supporting the mid-lower crustal flow model. However, these zones or bodies exhibit strong lateral heterogeneity in eastern Tibet, indicating a complex internal deformation process. The Sichuan Basin, which comprises the core of the Yangtze Craton, was subjected to long-term evolutionary processes following the Archaean, and it has been in a stable sedimentary environment since the Paleozoic. It is widely covered by Late Neoproterozoic to Phanerozoic shallow-marine and non-marine sedimentary strata. A thick lithosphere with high seismic velocities but little deformation was imaged beneath the Sichuan Basin, suggesting that this area has remained rigid and stable and has retained the characteristics of a typical craton (Bai et al., 2011; Zhang et al., 2010).

The nearly NE-trending LMS fault belt has long been enigmatic because of the abruptness of its terrain in addition to its low convergence rates and strong seismicity. It is mainly composed of three major faults, namely, the Maoxian–Wenchuan fault, the Beichuan–Yingxiu fault and the Pengxian–Guanxian fault. The LMS fault belt was originally formed during the Triassic Indo–Sinian orogeny. The Cenozoic continental collision reactivated this fault belt, forming the characteristically high topographic relief and the steepest slope along the eastern margin of the Tibetan Plateau. Thermochronologic data reveal that the growth of the high topography of eastern Tibet was the most rapid during two periods, namely, 25–30 and 10–15 million years ago (Wang et al., 2012). The LMS fault belt is dominated by dextral strike-slip faults with a significant thrust component (Burchfiel et al., 1995, 2008). Only very limited east–west shortening ($<3$ mm/yr) across the LMS fault belt has been detected from geodetic measurements (Shen et al., 2005) and geomorphic observations (Densmore et al., 2007). The present-day crustal thickness also demonstrates a symmetrical relationship with the topography; that is, it changes from $\sim$40 km beneath the Sichuan Basin to $\sim$60 km across the LMS fault belt beneath the Songpan–Ganzi block (Zhang et al., 2009, 2010).

Along the northern margin of central Tibet, the Kunlun fault, which follows the trace of the AKMS, represents one of the key tectonic boundaries in the scheme of Eurasian continental deformation. Accordingly, the AKMS exhibits a complex suturing history; the Qaidam and Kunlun blocks were sutured together during the Late Proterozoic and Paleozoic, after which they were collectively merged with the Songpan–Ganzi block during the Triassic (Yang et al., 1996). The Kunlun fault initiated as a sinistral strike-slip system at 15–8 Ma (Fu and Awata, 2007; Jolivet et al., 2003); it moves at rates from $>10$ mm/yr along its central-western part to $<2$ mm/yr along its easternmost part (Kirby et al., 2007). Previous geophysical studies also revealed substantial east–west differences in the crustal structure along the Kunlun fault; a Moho offset across the fault in the west (Vergne et al., 2002), but there is no obvious variation in the Moho depth in the east (Wang et al., 2011; Xu et al., 2014). Moreover, unequivocal seismic evidence has recently been collected, demonstrating that crustal LVZs have already partially penetrated northward across the Kunlun fault (Jiang et al., 2014). These east–west differences in the slip rate and crustal thickness along the Kunlun fault and the penetration of LVZs across the fault zone to the north suggest that the Kunlun fault plays a complex role in controlling the crustal deformation of northern and northeastern Tibet.

## 3. Data and methods

### 3.1. Data selection

The teleseismic data used in this study originated from 64 broadband seismic stations forming a linear array with an average station interval of 10–15 km (Fig. 1). The NW–SE-trending linear array starts in the southeast within the central Sichuan Basin and terminates in the northwest within the southern Qilian block. The 24 stations on the easternmost side were operated from November 2010 to November 2012 and the others were operated from September 2012 to September 2013. Three-component seismograms were selected from 1009 events with magnitudes $\geq$5.5 and epicentral distances between 28° and 92° (inset in Fig. 1). The waveforms were windowed from 20 s before to 100 s after the P-wave first arrival and then rotated from a vertical-north-east (ZNE) coordinate system to a vertical-radial-transverse (ZRT) coordinate system.

A P-wave receiver function is a time series that contains the structural response near the receiver. It is created by deconvolving the vertical component from the radial component to remove the instrument response in addition to the source and travel path information. We calculated the P-RFs using a time domain maximum entropy deconvolution method (Wu and Zeng, 1998). A Gaussian parameter of 3.0 and a water level of 0.001 were adopted for the deconvolution. After careful visual inspection, 14237 P-RFs with high signal-to-noise ratios have been selected, ensuring that the direct P-wave is clear and the *Ps* conversion from the Moho is distinguishable (Fig. 2).

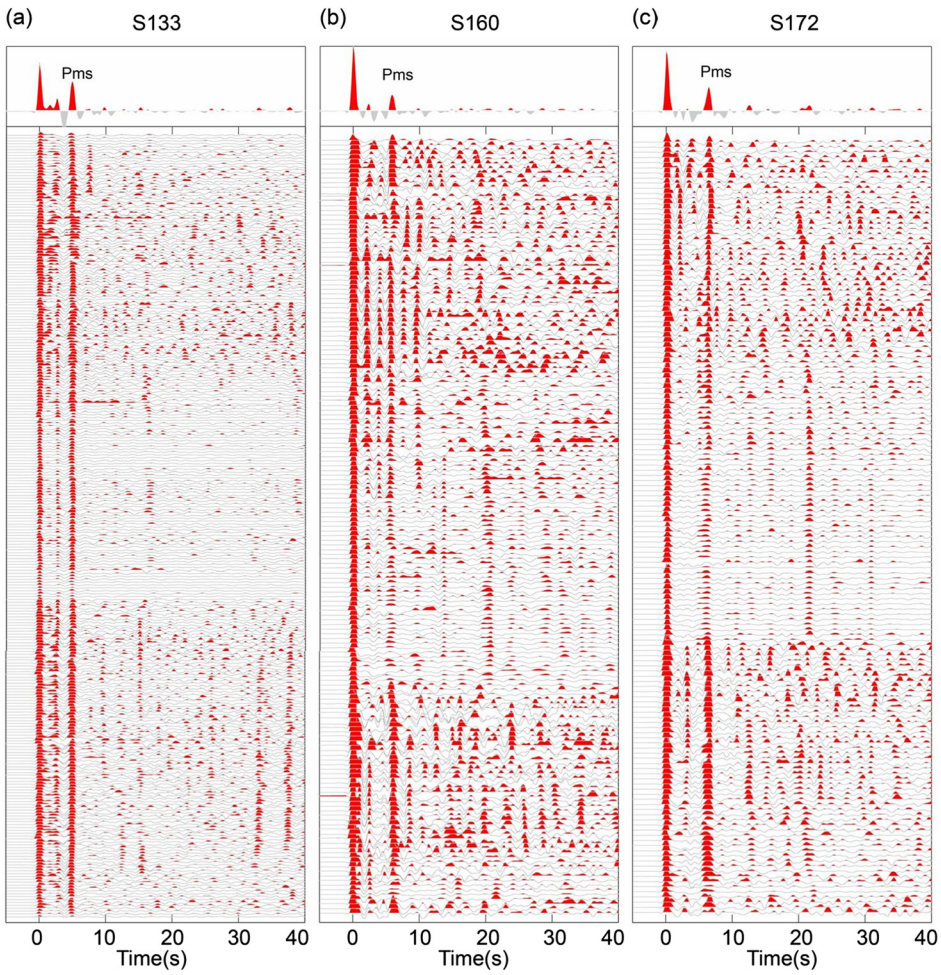


**Fig. 2.** Receiver functions at stations (a) S133, (b) S160 and (c) S172 located at the Sichuan Basin, the Songpan–Ganzi block and the Kunlun–West Qinling block, respectively (see Fig. 1 for station locations). All of the P-RFs were moveout-corrected to the case of vertical incidence, and plotted against back azimuth for each station. *Ps* conversions from the Moho (Pms) are clearly seen from almost all the individual traces and the summational traces in the top panels.

### 3.2. Wave-equation based migration technique

An image of the crustal discontinuity structure along the profile (A–A′ in Fig. 1) was constructed using a receiver function post-stack migration method consisting of two basic procedures: time-domain common conversion point (CCP) stacking of the P-RFs and spatial-domain backward wave field extrapolation. Backward wave field extrapolation is a migration process to project conversions to their true positions from the CCP stacked records at the surface. First, we calculated the *Ps* piercing points at the specified depths based on the one-dimensional regional velocity model. As the discontinuity depth is proportional to the delay time between the direct P phase and the converted *Ps* phase, receiver functions are more sensitive to the $Vp/Vs$ ratio than the absolute velocities above a discontinuity. Therefore, we considered the crustal $Vp/Vs$ ratio variation (see 3.3) when performing the moveout-corrections for all P-RFs to a vertical incidence as required for migration. Second, rectangular bins were used during the CCP stacking and its length perpendicular to the profile was maintained at each specified depth. The bin width parallel to the profile was allowed to vary with the data coverage to enhance the continuities of structural signals in areas with a sparse data coverage in addition to those for small structural features in areas with a dense data coverage. Finally, we backward propagated the stacked P-RFs from the surface to depths following the wave field extrapolation procedure for *Ps* conversions and constructed the image of the crustal structure in the frequency range of 0.01–1 Hz.

We also constructed the crustal structure images using multiples (i.e., $PpPs$ and $PpSs + PsPs$) reverberated between the free surface and velocity discontinuities in the crust and upper mantle. Multiples exhibit a much weaker sensitivity to the velocity structure than *Ps* conversions, and can therefore provide better constraints on the depths of subsurface discontinuities (Chen et al., 2006). To a large extent, the use of multiples can also bypass the interference from strong sedimentary reverberations within the effective signals from crustal discontinuities (Chen et al., 2006; Zheng et al., 2006). The same operation that performed for the *Ps* converted phases was also applied to the multiples. However, the moveout-correction of the P-RFs was performed according to the delay times of the multiples with respect to the direct P-wave arrival. The migration velocities for $PpPs$ are given by Chen et al. (2006); meanwhile, for $PsPs + PpSs$, the following equation was used instead of that for *Ps* (Chen et al., 2005, equation (13)) in migration:

$$V_{PsPs+PpSs}(x, z) = V_S(x, z)/2 \tag{1}$$

### 3.3. H–K stacking technique

We used the H–K stacking technique for receiver functions to extract the crustal thickness (H) and $Vp/Vs$ ratio (K) under each station, as exemplified in Fig. 3. This method is performed by searching for the most energetic stack consisting of the first con-

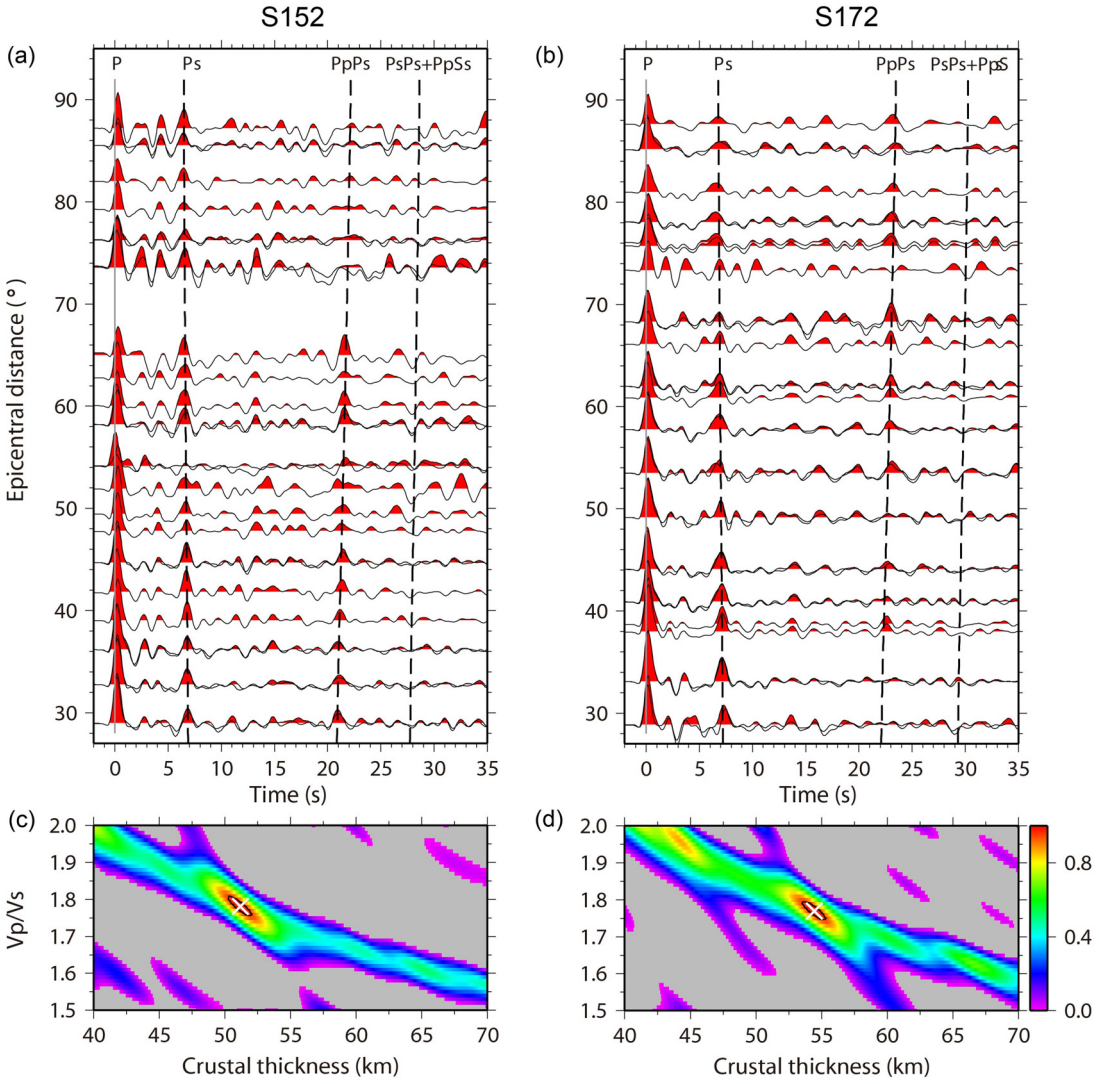


**Fig. 3.** Receiver functions sorted by epicentral distance (a), (b) and H–K stacking results (c), (d) for representative stations. Station S152 (a), (c) is located in the Songpan–Ganzi block and station S172 (b), (d) in the Kunlun–West Qinling block (see Fig. 1 for station locations). Black dashed lines in the upper panels show the theoretical arrival times of the first converted phase and the multiple phases from the Moho, which are derived from the optimal model. The lower panels illustrate the distribution of the normalized stacking amplitudes, the white crosses represent the best estimates of crustal thickness and $Vp/Vs$ ratio, and the black ellipses show the 95% confidence intervals.

verted phase and the two multiple phases from the Moho based on their delay times relative to the direct P-wave arrival time predicted using a model with a single crustal homogeneous layer. In this study, a regional average crustal $Vp$ of 6.3 km/s was adopted from wide-angle reflection and refraction (WAR/R) studies (Zhang et al., 2011) for the calculation. To emphasize arrivals of the $Ps$ phase, the amplitudes of the $Ps$, $PpPs$ and $PpSs + PsPs$ phases were summed with weights of 0.7, 0.2 and 0.1, respectively. The grid searching was performed within the range of 40–70 km for H and 1.5–2.0 for $Vp/Vs$ (Figs. 3c and 3d). Because of the presence of high noise levels or complex crustal structures under some of the stations, multiple peaks that make the results ambiguous can be observed in the solution surfaces constructed during the H–K stacking. Instead of discarding these results, we chose the peaks that were consistent with the results obtained for nearby stations. After a visual inspection of the P-RFs, only the result for one station was discarded due to its great disparity and poor data quality.

## 4. Result and interpretation

The migrated images constructed using the $Ps$, $PpPs$ and $PsPs + PpSs$ phases are respectively shown in Figs. 4b, 4c and 4d. Considering the large topographic relief along the image profile (Fig. 4a), all of the migrated images have been corrected to the sea level datum. In the $Ps$ image (Fig. 4b), the Moho is detected as a strong positive converted phase at depths from 40 to 60 km. The images constructed from the multiples (Figs. 4c and 4d) provide Moho depths that are consistent with the $Ps$ image, suggesting that the Moho depths are reliable and little affected by the low velocities of surface sediments.

### 4.1. Moho fluctuation beneath individual tectonic units

The Moho effectively mirrors the surface topography along the profile and exhibits obvious offsets near tectonic boundary zones. We divided the imaging profile into three units based on the tectonic subdivision of the study region and the lateral variations of the Moho depth as imaged. From northwest to southeast, the three units are the Kunlun–West Qinling block (northwest of the AKMS/Kunlun fault), the Songpan–Ganzi block (in between the AKMS/Kunlun fault and the LMS fault belt), and the Sichuan Basin (including the LMS fault belt and the area to the southeast).

As shown in Figs. 4b–d, the Kunlun–West Qinling block is characterized by a slightly northwest-dipping Moho (from ~51 km to

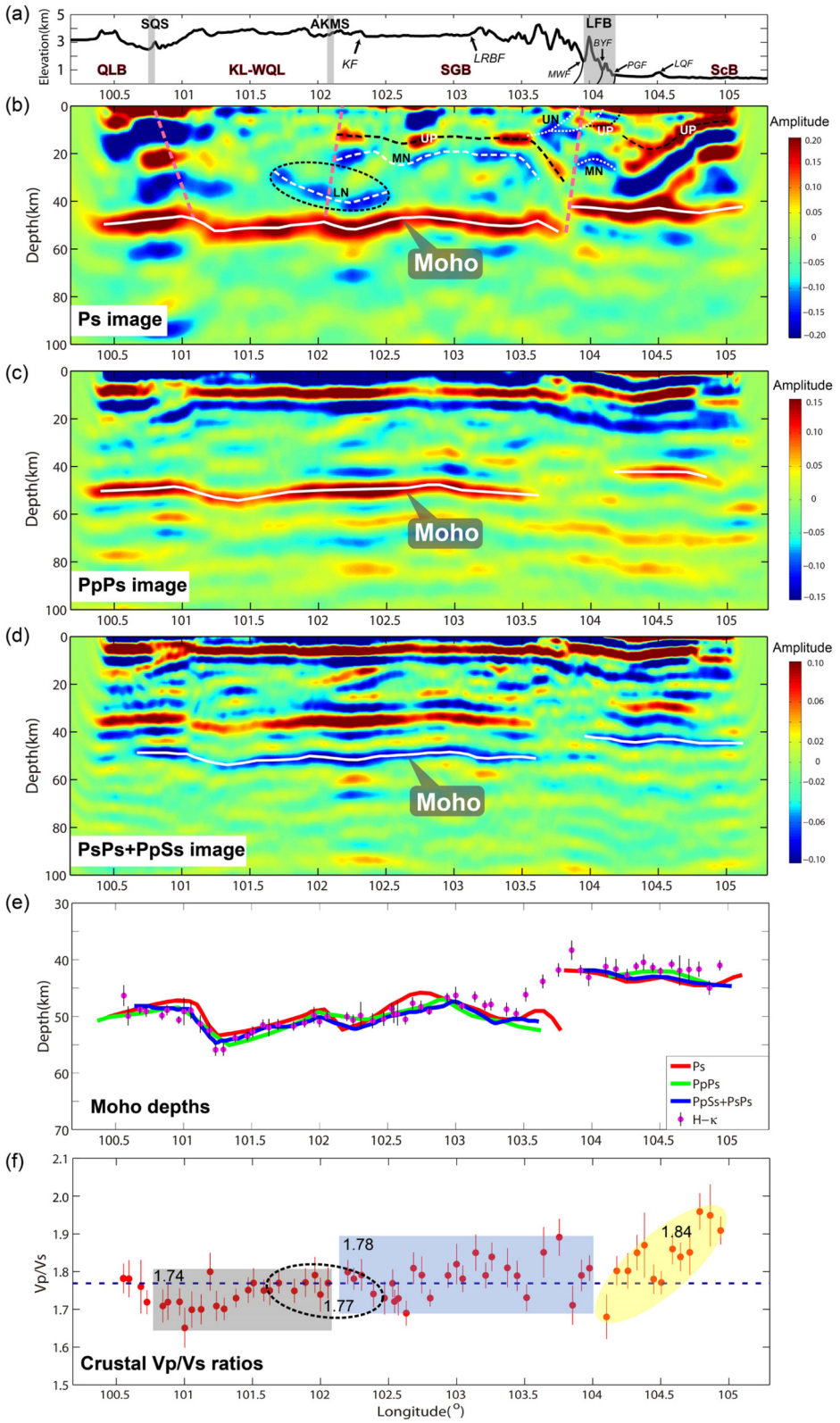


**Fig. 4.** Surface topography (a), migrated P-RF images (b)–(d), estimated Moho depths (e) and crustal $Vp/Vs$ ratios (f) along profile A–A′. The migrated images are constructed using $Ps$ phases with frequencies of 0.01–1 Hz (b), using $PpPs$ with frequencies of 0.03–0.3 Hz (c) and $PsPs + PpSs$ multiples with frequencies of 0.01–0.3 Hz (d), respectively. In the $Ps$ image (b), intracrustal positive and negative discontinuities are delineated by black dashed lines and white dashed lines, respectively; Pink dashed lines mark the block boundary. White lines in (b)–(d) depict the geometry of the Moho. The Moho depths shown in (e) are estimated from the migrated images (b)–(d) and the H–$\kappa$ stacking results (see text). The average crustal $Vp/Vs$ ratios beneath individual stations in (f) are projected onto the imaging profile (red circles represent the $Vp/Vs$ ratio, with line segments being its error bars). The ellipses of the black dashed line in (a) and (f) mark an anomaly region, where both a lower-crustal negative discontinuity and a high crustal $Vp/Vs$ ratio of ~1.77 exist. Abbreviations in (a): QLB, Qilian block; KL–WQL, Kunlun–West Qinling block; SGB, Songpan–Ganzi block; ScB, Sichuan Basin; AKMS, Anyimaqen–Kunlun–Muztagh suture; SQS, South Qilian suture; KF, Kunlun fault; LFB, Longmenshan fault belt; PGF, Pengxian–Guanxian fault; BYF, Beichuan–Yingxiu fault; MWF, Maoxian–Wenchuan fault; LRBF, Longriba fault; LQF, Longquan fault. Abbreviations in (b): UP, upper-crustal positive signal; UN, upper-crustal negative signal; MN, mid-crustal negative signal; LN, lower-crustal negative signal.

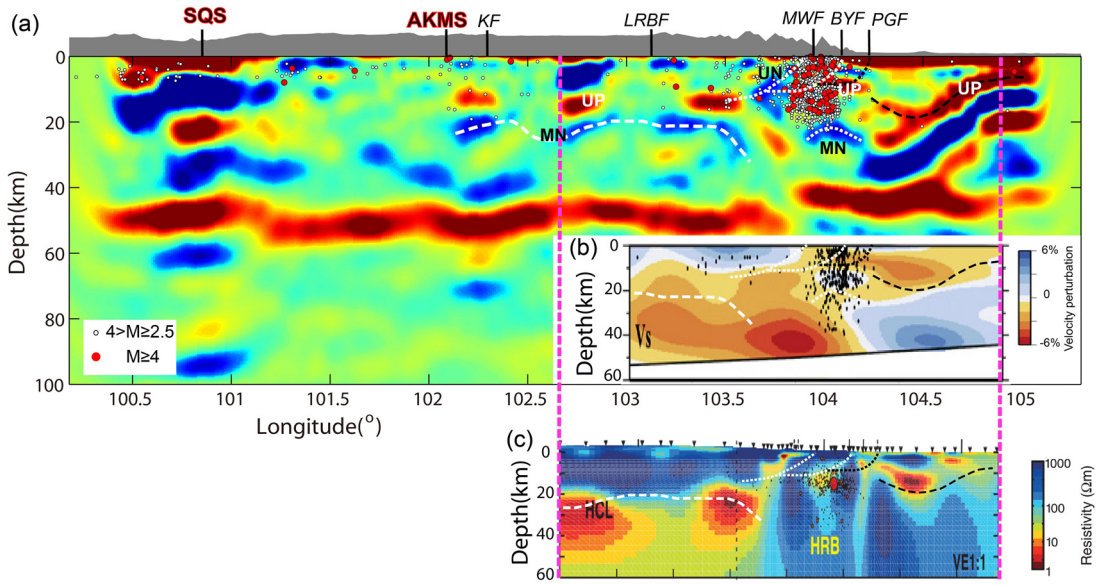


**Fig. 5.** Comparison of the *Ps* image (a) with the tomographic image (b, Wang et al., 2014) and the MT data (c, Zhao et al., 2012) beneath eastern Tibet. Locations of the tomographic imaging section (b) and the MT stations (c) are shown in Fig. 1. The black and the white dashed lines, denoting the positive and the negative discontinuities extracted from the *Ps* image respectively, are also marked in (b) and (c). Solid circles in (a) represent the locations of the earthquakes occurred between October 2008 and September 2016, which are within 50 km from the migration profile. Abbreviations in (a): AKMS, Anyimaqen–Kunlun–Muztagh suture; SQS, South Qilian suture; KF, Kunlun fault; LRBF, Longriba fault; PGF, Pengxian–Guanxian fault; BYF, Beichuan–Yingxiu fault; MWF, Maoxian–Wenchuan fault; UP, upper-crustal positive signal; UN, upper-crustal negative signal; MN, mid-crustal negative signal. Abbreviations in (c): HCL, high conductivity layer; HRB, high resistivity body.

~56 km). An obvious Moho offset appears at ~101.1°E near the South Qilian suture; this offset may be indicative of a deep suture boundary between the Kunlun–West Qinling block and the Qilian block. Our observations show a weak Moho variation (~3 km) at ~102°E near the Kunlun fault, which is similar to a 2–5 km Moho offset reported from previous deep seismic soundings (Zhang et al., 2011) and is even correlative with the lack of Moho undulations observed during recent active and passive source seismic imaging (Wang et al., 2011; Xu et al., 2014). Further to the southeast, an arched Moho is detected with the minimum depth of ~49 km beneath the central-northwestern part of the Songpan–Ganzi block along the profile and the maximum depth of ~55 km on either side.

The Moho beneath the Sichuan Basin and the LMS area is continuous and nearly flat (~43 km), which strongly suggests that the crystalline crust beneath the LMS area is probably of Yangtze origin (Burchfiel et al., 1995; Yin and Harrison, 2000). Therefore, we consider the LMS area as a marginal part of the Yangtze Craton. A dramatic Moho offset ~10 km appears at the eastern margin of the Songpan–Ganzi block, consistent with the result of Zhang et al. (2009). This offset may mark the deep boundary between the Yangtze Craton and the Tibetan Plateau.

### 4.2. Intracrustal discontinuities

Besides the Moho, both positive and negative signals with clear but intermittent characteristics also appear in our *Ps* image (Fig. 4b). Some of them, especially those at either side of our profile, may be substantially interfered by strong sediment reverberations. However, after systematic tests (Figs. S1–S3) and comparisons with previous studies, the signals marked in Fig. 4b are considered as real discontinuities.

The upper-crustal positive (UP) signals are strongly intermitted and change dramatically in depths along the profile (Fig. 4b). They should be real and represent the top interface of the basement (the crystalline crust) in virtue of their striking similarity in both locations and depths with the shallow strong reflectors in recent deep seismic reflection profiles (Gao et al., 2016; Guo et al., 2013). The top interface of the basement lies flat at ~14–16 km depths beneath the main part of the Songpan–Ganzi block and dramatically dips eastward to the Moho offset at the eastern margin of the block. The top interface of the basement in the LMS area is evident within the *Ps* image as a strong horizontal discontinuity at a depth of ~10 km. This discontinuity may be associated with a major detachment connecting both the Beichuan–Yingxiu fault and the Pengxian–Guanxian fault (Guo et al., 2013; Hubbard and Shaw, 2009). From the LMS tectonic belt to the Sichuan Basin, the top interface of the basement deepens from ~15 km around the basin-mountain boundary to ~18 km near the Longquan fault, after which the interface shallows to ~6 km beneath the central Sichuan Basin.

The mid-crustal negative (MN) and the lower-crustal negative (LN) signals beneath eastern and northeastern Tibet are a little weak and relatively close to the UP and the Moho signals, respectively. Therefore, we did a series of tests to explore these signals (see details in the supplementary material). We found that these signals show much weaker time-shifts with frequency than predicted with the side-lobe (Fig. S1). Moreover, these signals can be traced and exhibit similar features not only in the time-domain CCP stacking sections using different smoothing schemes (Fig. S2) but also in the images with different back azimuths of data (Fig. S3). These tests largely exclude the possibility of side-lobe, noise, local scattering or noticeable anisotropy for the origin of these signals, supporting that they represent real discontinuities.

The MN discontinuity lies at ~20–25 km depths beneath the main part of the Songpan–Ganzi block and dips up to ~30 km depth towards the east at the eastern margin of the block. It is not equally strong along the profile, being weaker or even invisible near the area of the Longriba fault (Fig. 5a). This feature corresponds well with the laterally heterogeneous structure of the high-conductivity layer, which appears to be less conductive around the Longriba fault compared with the much higher conductivities on either side (Fig. 5c; Zhao et al., 2012). Additionally, this discontinuity is also in accordance with the upper boundary of the low-velocity mid-lower crust in eastern Tibet revealed by the tomographic result (Fig. 5b; Wang et al., 2014). Thus, it may

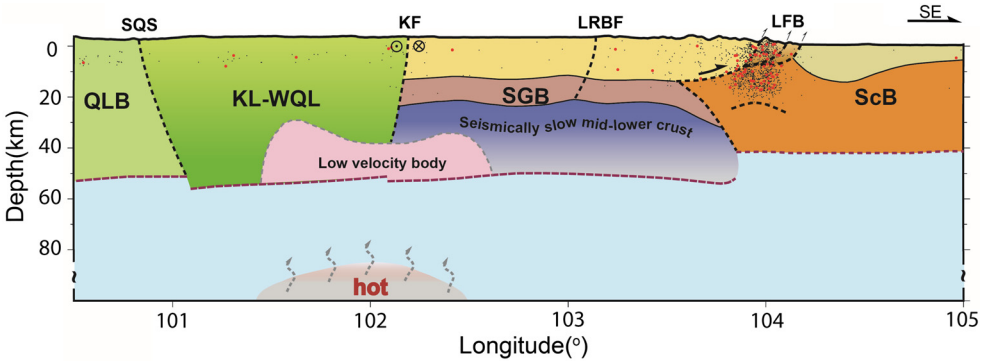


**Fig. 6.** Crustal model of eastern and northeastern Tibet based on the crustal discontinuities identified from our P-RF migrated images. Black dashed lines represent major faults and crustal-scale boundaries between tectonic blocks. Purple dashed lines mark the crust–mantle boundary, i.e., the Moho. Earthquakes within 50 km from the profile are shown as dots. Black and red solid dots are earthquakes with magnitudes 2.5–4.0 and ≥4.0 that occurred from October 2008 to September 2016, respectively. Faults are delineated mainly based on the previous seismic reflection studies (Hubbard and Shaw, 2009; Li et al., 2010; Guo et al., 2013; Wang et al., 2011). High temperatures in the lower crust and upper mantle right beneath the Kunlun fault are deduced based on the low seismic velocities constrained from surface wave observation (Li et al., 2016). QLB: Qilian block; KL–WQL: Kunlun–West Qinling block; SGB: Songpan–Ganzi block; ScB: Sichuan Basin; SQS: South Qilian suture; KF: Kunlun fault; LFB: Longmenshan fault belt; LRBF: Longriba fault.

represent the upper boundary of the seismically slow and highly conductive mid-lower crust.

The LN discontinuity crosses the Kunlun fault and is concave downwards at depths of 30–40 km (Fig. 4b). Recent seismic studies revealed a mid-lower crustal low-velocity anomaly close to where the LN discontinuity appeared, which also crossed the Kunlun fault (Jiang et al., 2014; Li et al., 2016; Wu et al., 2018). Therefore, we interpret the LN discontinuity as the upper boundary of the low-velocity body in the lower crust.

The upper-crustal negative (UN) signal at the eastern margin of the Songpan–Ganzi block decreases from 12–15 km depths to near the surface. It may represent a detachment zone associated with nappe structures in eastern Tibet (Hubbard and Shaw, 2009; Li et al., 2010).

The MN signal beneath the LMS area appears at a depth of ~25 km. It obviously differs in the morphology from the UP discontinuity above. Moreover, its travel-time does not agree with that of the multiple predicted with the UP discontinuity. Considering these features and comparing with previous studies, we infer that this MN signal is not the multiple from the shallow interface but probably reflects a high-velocity upper crust (Pei et al., 2010; Wang et al., 2014).

### 4.3. Crustal lithologies of individual tectonic units

Despite an obvious disparity at 103.5–103.8°E, where the crustal structure appears the most complicated along the imaging profile, the Moho depths from the H–K stacking results and the migrated images of P-RFs are highly consistent with each other (Fig. 4e). Such a consistency also increases the reliability of the crustal $Vp/Vs$ ratios obtained from individual seismic stations.

The resulting $Vp/Vs$ values show a general decrease from the southeast to the northwest along the imaging profile (Fig. 4f). This result is in agreement with most previous estimates of the crustal $Vp/Vs$ ratios (Wei et al., 2016; Xu et al., 2014). The western Sichuan Basin exhibits the highest crustal $Vp/Vs$ ratios (1.68–1.96 with an average of 1.84). In contrast, the Kunlun–West Qinling block is characterized by the lowest crustal $Vp/Vs$ ratios (1.65–1.80 with an average of 1.74). Moreover, the southern portion of the Kunlun–West Qinling block shows higher $Vp/Vs$ ratios (1.74–1.80 with an average of 1.77) than its northern section (1.65–1.80 with an average of 1.72) and northeastern Tibet (~1.72; Tian and Zhang, 2013). The Songpan–Ganzi block shows normal to relatively high crustal $Vp/Vs$ ratios (1.69–1.89 with an average of 1.78).

The value of $Vp/Vs$ ratio is closely related with the mineralogy and chemical composition of the crust, and often taken as an indicator of partial melting, a process which tends to significantly raise the $Vp/Vs$ ratios (Watanabe, 1993). Christensen (1996) concluded that a continental crust comprising felsic, intermediate and mafic lithologies would have low ($<$1.76), medium (1.76–1.81) and high ($>$1.81) velocity ratios, respectively, in accordance with comprehensive results from laboratory experiments. Within the Sichuan Basin, the $Vp/Vs$ ratio is not positively correlated with the sedimentary thickness observed in the $Ps$ image (Figs. 4b and 4f), probably suggesting that the crystalline crust of the Sichuan Basin mainly contributes to the significantly high ratio and is more mafic in composition. In contrast, a low $Vp/Vs$ ratio (~1.74) from the Kunlun–West Qinling block and a moderate value (~1.78) from the Songpan–Ganzi block are probably associated with bulk felsic and intermediate crustal compositions, respectively.

## 5. Discussion

The crustal discontinuities identified from our migrated images allow us to construct a regional crustal structure model along the target profile (shown in Fig. 6). To better understand the crustal structure and associated deformation, major faults are delineated based on previous seismic reflection studies (Guo et al., 2013; Hubbard and Shaw, 2009; Li et al., 2010; Wang et al., 2011) and earthquakes within 50 km from the image profile are also projected. In this section, we analyse and compare the crustal properties and structures of the three tectonic units, and further discuss the crustal deformation and its implication for the tectonic evolution of eastern and northeastern Tibet.

### 5.1. Crustal deformation and crustal flow

The Tibetan Plateau comprises a complex amalgamation of blocks with different ages, and it was subjected to significant crustal thickening and topographic uplift during the Cenozoic (Tapponnier et al., 2001; Yin and Harrison, 2000). The collision of the Tibetan Plateau with the Yangtze Craton and the resulting northeastward extrusion significantly affected the crustal structure and deformation of the Songpan–Ganzi block. The crustal properties and structures of this block and its adjacent blocks constitute the basis for reconstructing the processes of plateau uplift and expansion. The structures and lithologies of the crust along our imaging profile reflect significant differences in the crustal strength and deformations of individual blocks.

The nearly flat and shallow Moho suggests that the crystalline crust of the Sichuan Basin may have been little deformed, due probably to its mafic lithology and rigid property. The large variation in the basal depth of the sediments within the Sichuan Basin does not affect the crust–mantle boundary, implying that the lateral variation could be more related to the Neoproterozoic–Mesozoic uplift or modification (Mei et al., 2014) than to the Cenozoic Indian–Eurasian collision. The rigid property of the Sichuan Basin has also been revealed by Zhang et al. (2009) along a profile ~100 km to the south of ours, as the basin crust is obviously thin. However, in the western Sichuan Basin and the LMS area, the Moho depth variation and the $Vp/Vs$ ratios we observed slightly differ from that Zhang et al. (2009) revealed. This probably reflects a north-south variation of the crustal structure and properties along the LMS tectonic belt (Li et al., 2010; Mei et al., 2014; Pei et al., 2010; Wang et al., 2014).

The Tibetan crust is imaged to be thicker and felsic-intermediate in composition with obvious lateral variations, indicating that it has been subjected to severe deformation. The Kunlun–West Qinling block does not show any strong intracrustal discontinuity, which may be indicative of smooth vertical gradients of the crustal velocity structure. The crust of this block is felsic in composition, supporting that the crustal deformation is predominated by the upper-crustal thickening in northeastern Tibet (Tian and Zhang, 2013; Xu et al., 2014). The crust of the Songpan–Ganzi block, in contrast, exhibits a better vertical stratification. The two nearly parallel discontinuities with opposite polarities divide the crust of the Songpan–Ganzi block into three layers, namely, a low-velocity sedimentary layer, a thin upper crust and a seismically slow mid-lower crust (Fig. 6). The crustal stratified structure, however, is laterally inhomogeneous, consistent with recent studies in eastern Tibet (Guo et al., 2013; Liu et al., 2017; Zhao et al., 2012). This probably suggests that the crust deforms with strong lateral differences in this area.

When combined with MT studies and GPS data, the low-velocity mid-lower crust and relatively high $Vp/Vs$ ratio of the Songpan–Ganzi block, to some extent, supports the existence of channelized crustal flow in this area. Both the seismic and MT images (Fig. 5) suggest that the crustal flow may be laterally inhomogeneous or spatially localized, and probably is confined by large faults such as the LMS fault belt and the Kunlun fault. A recent study around the Ruoergai Basin (Liu et al., 2017) suggested that large strike-slip faults, rather than the crustal flow, contributed greatly to the plateau expansion and uplift in eastern Tibet. This further supports that the crustal flow is spatially localized, and the crustal deformation is diversified in eastern Tibet. However, no matter what mechanism dominates the crustal deformation in this area, the large faults should be always of vital importance in the plateau uplift and expansion.

### 5.2. Wedging tectonics beneath the LMS area

The LMS area, which is characterized by dramatic topographic relief and strong seismicity, inspired a vigorous debate regarding the process through which the uplift was produced and maintained. Geodynamic models, including upper crustal detachments (Hubbard and Shaw, 2009), crustal channel flow (Royden et al., 1997) and wedging tectonics (Cai et al., 1996), have been proposed to explain these phenomena.

Previous studies suggested that a series of faults in the LMS area formed a nappe structure in the upper crust (Hubbard and Shaw, 2009; Li et al., 2010), where we observed an obvious negative discontinuity in the $Ps$ image. Our new observations also provide more constraints on the mid-lower crustal structures, such as the east-dipping positive discontinuity in the $Ps$ image marking the deep contact boundary between the Yangtze Craton and Tibet. This crustal architecture in the LMS area is consistent with that imaged ~100 km to the south (Zhang et al., 2009), thereby suggesting a large-scale structural feature along the LMS fault belt, at least in its central-southern segment where the reverse thrust is dominant. Our new seismic images in combination with results from previous studies suggest that the rigid, crystalline crust of the Sichuan Basin may have been wedged into the crust beneath eastern Tibet, leading to an eastward overthrusting of the Tibetan shallow crust onto the Yangtze Craton accompanying a thickening of the rheologically deformable mid-lower crust in this area. Thermochronologic data show that the high topography in eastern Tibet experienced a two-phase growth during the Cenozoic (Wang et al., 2012). This indicates that perhaps the brittle upper crust and the ductile mid-lower crust contribute during two different geological periods to the crustal thickening and plateau uplift in this area.

The wedging tectonics may play a key role in seismogenesis in the LMS area. The earthquakes are mainly distributed in the high-velocity upper crust of the LMS area, where the crust is obviously thin; this likely suggests that stresses are mostly released by the fracturing of rocks rather than uniform crustal thickening. The upper crust of violent breaking may be mechanically decoupled from its underlying part, as the lower crust is relatively weaker than the upper crust in the central segment of the LMS fault belt (Wang et al., 2014). The Songpan–Ganzi block, to the west of the LMS area, plays the role of a stress transmitter to the LMS area (Guo et al., 2013) and partially absorbs those stresses through vertical crustal deformation.

### 5.3. Lowermost crust modification around the easternmost Kunlun fault by mantle upwelling

Many geophysical studies of the crustal structure and properties have been conducted across the Kunlun fault in recent years (Jiang et al., 2014; Pape et al., 2012; Wang et al., 2011; Xu et al., 2014; Zhang et al., 2011). The results of these studies show that the role of the Kunlun fault on the regional crustal and lithospheric deformation is highly complex.

In our seismic images, the undulation of the Moho and the clear-cut difference in the intracrustal structure across the Kunlun fault (Figs. 4b–d) suggest that the crust of the Kunlun–West Qinling block is in sharp contact with that of the Songpan–Ganzi block. Additionally, a low-velocity body appears just above the Moho, and the Kunlun fault seems to be merging with it at depths of ~35–40 km. The maximum velocity drop marking the top surface of the crustal flow channel beneath the Songpan–Ganzi block appears at a depth of ~25 km and exhibits a nearly flat geometry (Figs. 4b and 5). The low-velocity body beneath the Kunlun fault is remarkably different from the channelized flow in terms of both the shape and depths. Perhaps this low-velocity body formed with a different mechanism. Here, we conclude that this low-velocity body could be attributable to partial melting induced by elevated temperature based on the following points. (1) The $Vs$ of the low-velocity body close to where the LN discontinuity appears (3.2–3.4 km/s; Wang et al., 2017; Wu et al., 2018) is lower than the $Vs$ when the dry metamorphic rock at 30 km depth is at melting point (3.4 km/s, Litvinovsky et al., 2000). (2) The low-velocity body has an abnormally high $Vp/Vs$ ratio of ~1.88 by calculation (Fig. S5), which is considered to be related to the process of partial melting (Watanabe, 1993).

The origin of this low-velocity is of great significance to understand the process of crustal deformation along the Kunlun fault. The slip along the Kunlun fault probably drove the internal deformation, namely the crustal thickening, surrounding the fault tip (Kirby et al., 2007). However, the present-day crustal thickness around the eastern tip of the Kunlun fault is similar to, even thin-

ner than that of its surroundings, as observed in this and previous studies (Xu et al., 2014; Wang et al., 2011). It may indicate a removal of eclogitic crust before (Wang et al., 2017). The slip rate is much lower at the eastern tip of the Kunlun fault (Kirby et al., 2007), so shear heating resulted from the relative movement across the fault should be too limited to cause melting. Li et al. (2016) observed a low-velocity lithosphere with negative radial anisotropy and significant low-velocities below with positive radial anisotropy right beneath the eastern part of the Kunlun fault. They suggested the presence of a localized asthenospheric upwelling following the delamination of a thick lithospheric root. This scenario is also supported by the relatively high heat flow (Jiang et al., 2016) and rapid rock uplift (Kirby and Harkins, 2013). Thus, the low-velocity anomaly that we observed beneath the easternmost Kunlun fault area might represent a deep-crustal response to the lithospheric delamination-induced localized asthenospheric upwelling.

## 6. Conclusions

Applying a wave-equation poststack migration technique to P-RFs extracted from a dense seismic array, we constructed new crustal structural images for the eastern and northeastern Tibetan region. Our results show that individual tectonic blocks in the study region exhibit significant differences in average crustal $Vp/Vs$ ratio, Moho depth and intracrustal structure. These differences suggest that the crust of these tectonic blocks probably have different natures and thus different responses to the Cenozoic continental collision. The crust of the Kunlun–West Qinling block and the Songpan–Ganzi block may have been subjected to noticeable thickening and weakening, while the crystalline crust of the Sichuan Basin little deformed due to its rigidity inherited from the Yangtze Craton.

Combined with previous studies, our observations suggest that the crustal shortening in east and northeast Tibet may have been absorbed by not only vertical thickening in the interiors of the tectonic blocks but also complex local deformation along the boundary zones. Our results reveal the presence of channelized crustal flow in the Songpan–Ganzi block, which is characterized by a weak connectivity and controlled by large faults. Along the boundary zones, the rigid crust of the Sichuan Basin might have wedged into the Tibetan crust in the LMS area, and the Kunlun fault could have acted as a focus of heating and hot mantle upwelling associated with the deep processes of the Indian plate underthrusting and subduction.

## Acknowledgements

We acknowledge the participants of the Seismic Array Laboratory of IGGCAS for collecting the data. We thank Weijun Wang at the Institute of Earthquake Forecasting, China Earthquake Administration for providing the earthquake hypocenter data, Yang Shen and two anonymous reviewers for their constructive comments and suggestions. This research is supported by the National Natural Science Foundation of China (Grant No. 41688103), the Project SKL-Z201704-11712180, and the International Partnership Program (GJHZ1776) of the Chinese Academy of Sciences. The field work for seismic data collection was financially supported by the Projects 2011ZX05008-001 and SinoProbe-02-03. L.C. thanks the hospitality of COFFICE at IGGCAS.

## Appendix A. Supplementary material

Supplementary material related to this article can be found online at https://doi.org/10.1016/j.epsl.2018.06.007.

## References

Bai, Z., Tian, X., Tian, Y., 2011. Upper mantle P-wave tomography across the Longmenshan fault belt from passive-source seismic observations along Aba–Longquanshan profile. J. Asian Earth Sci. 40 (4), 873–882.

Burchfiel, B.C., Chen, Z., Liu, Y., Royden, L.H., 1995. Tectonics of the Longmenshan and adjacent regions. Int. Geol. Rev. 37, 661–735.

Burchfiel, B.C., Royden, L.H., van der Hilst, R.D., Hager, B.H., Chen, Z., King, R.W., Li, C., Lü, J., Yao, H., Kirby, E., 2008. A geological and geophysical context for the Wenchuan earthquake of 12 may 2008, Sichuan, People's Republic of China. GSA Today 18 (18), 4–11.

Cai, X.L., Wei, X.G., Liu, Y.C., Cao, J.M., 1996. On wedge-in orogeny – on the example of the Longmenshan orogenic belt. Acta Geol. Sichuan 16, 97–102 (in Chinese with English abstract).

Chen, L., Wen, L., Zheng, T., 2005. A wave equation migration method for receiver function imaging: 1. Theory. J. Geophys. Res. 110, B11309. https://doi.org/10.1029/2005JB003665.

Chen, L., Zheng, T., Xu, W., 2006. Receiver function migration image of the deep structure in the Bohai Bay Basin, eastern China. Geophys. Res. Lett. 33, L20307. https://doi.org/10.1029/2006GL027593.

Christensen, N.I., 1996. Poisson's ratio and crustal seismology. J. Geophys. Res. 101, 3139–3156. https://doi.org/10.1029/95JB03446.

Densmore, A.L., Ellis, M.A., Li, Y., Zhou, R., Hancock, G.S., Richardson, N., 2007. Active tectonics of the Beichuan and Pengguan faults at the eastern margin of the Tibetan Plateau. Tectonics 26, TC4005. https://doi.org/10.1029/2006TC001987.

Fu, B., Awata, Y., 2007. Displacement and timing of left-lateral faulting in the Kunlun Fault Zone, northern Tibet, inferred from geologic and geomorphic features. J. Asian Earth Sci. 29, 253–265.

Gao, R., Chen, C., Wang, H., Lu, Z., Brown, L., Dong, S., Feng, S., Li, Q., Li, W., Wen, Z., Li, F., 2016. SINOPROBE deep reflection profile reveals a Neo-Proterozoic subduction zone beneath Sichuan Basin. Earth Planet. Sci. Lett. 454 (18), 86–91.

Guo, X., Gao, R., Keller, G.R., Xu, X., Wang, H., Li, W., 2013. Imaging the crustal structure beneath the eastern Tibetan Plateau and implications for the uplift of the Longmen Shan range. Earth Planet. Sci. Lett. 379 (5), 72–80.

Hubbard, J., Shaw, J.H., 2009. Uplift of the Longmenshan and Tibetan Plateau, and the 2008 Wenchuan (M = 7.9) earthquake. Nature 458, 194–197. https://doi.org/10.1038/nature07837.

Jiang, C.X., Yang, Y.J., Zheng, Y., 2014. Penetration of mid-crustal low velocity zone across the Kunlun Fault in the NE Tibetan Plateau revealed by ambient noise tomography. Earth Planet. Sci. Lett. 406 (3), 81–92.

Jiang, G.Z., Gao, P., Rao, S., Zhang, L.Y., Tao, X.Y., Huang, F., Zhao, P., Pang, Z.H., He, L.J., Hu, S.B., Wang, J.Y., 2016. Compilation of heat flow data in the continental area of China (4th edition). Chin. J. Geophys. 59 (8), 2892–2910. https://doi.org/10.6038/cjg20160815 (in Chinese).

Jolivet, M., Brunel, M., Seward, D., Xu, Z., Yang, J., Malavieille, J., Roger, F., Leyreloup, A., Arnaud, N., Wu, C., 2003. Neogene extension and volcanism in the Kunlun Fault Zone, northern Tibet: new constraints on the age of the Kunlun Fault. Tectonics 22, 1052. https://doi.org/10.1029/2002TC001428.

Kirby, E., Harkins, N., Wang, E., Shi, X., Fan, C., Burbank, D., 2007. Slip rate gradients along the eastern Kunlun fault. Tectonics 26 (2), 485–493.

Kirby, E., Harkins, N., 2013. Distributed deformation around the eastern tip of the Kunlun fault. Int. J. Earth Sci. 102 (7), 1759–1772.

Li, L., Li, A., Murphy, M.A., Fu, Y.V., 2016. Radial anisotropy beneath northeast Tibet, implications for lithosphere deformation at a restraining bend in the Kunlun fault and its vicinity. Geochem. Geophys. Geosyst. 17, 3674–3690. https://doi.org/10.1002/2016GC006366.

Li, Y.Q., Jia, D., Shaw, J.H., Hubbard, J., Lin, A.M., Wang, M.M., Luo, L., Li, H.B., Wu, L., 2010. Structural interpretation of the coseismic faults of the Wenchuan earthquake. Three-dimensional modeling of the Longmen Shan fold-and-thrust belt. J. Geophys. Res. 115, B04317. https://doi.org/10.1029/2009JB006824.

Litvinovsky, B.A., Steele, I.M., Wickham, S.M., 2000. Silicic magma formation in overthickened crust: melting of charnockite and leucogranite at 15, 20 and 25 kbar. J. Petrol. 41 (5), 717–737.

Liu, Q.Y., van der Hilst, R.D., Li, Y., Yao, H.J., Chen, J.H., Guo, B., Qi, S.H., Wang, J., Huang, H., Li, S.C., 2014. Eastward expansion of the Tibetan Plateau by crustal flow and strain partitioning across faults. Nat. Geosci. 7 (5), 361–365. https://doi.org/10.1038/ngeo2130.

Liu, Z., Tian, X.B., Gao, R., Wang, G.C., Wu, Z.B., Zhou, B.B., Tan, P., Nie, S.T., Yu, G.P., Zhu, G.H., Xu, X., 2017. New images of the crustal structure beneath eastern Tibet from a high-density seismic array. Earth Planet. Sci. Lett. 480, 33–41. https://doi.org/10.1016/j.epsl.2017.09.048.

Mei, Q.H., He, D., Wen, Z., Li, Y., 2014. Geologic structure and tectonic evolution of Leshan–Longnvsi paleo-uplift in Sichuan Basin, China. Acta Petrol. Sin. 35 (1), 11–25.

Nie, S., Yin, A., Rowley, D.B., Jin, Y., 1994. Exhumation of the Dabie Shan ultrahighpressure rocks and accumulation of the Songpan–Ganzi flysch sequence, central China. Geology 22, 999–1002.

Pape, F.L., Jones, A.G., Vozar, J., Wei, W., 2012. Penetration of crustal melt beyond the Kunlun fault into northern Tibet. Nat. Geosci. 5 (5), 330–335.

Pei, S.P., Su, J.R., Zhang, H.J., Sun, Y.S., Toksöz, M.N., Wang, Z., Gao, X., Zeng, J.L., He, J.K., 2010. Three-dimensional seismic velocity structure across the 2008 Wenchuan Ms 8.0 earthquake, Sichuan, China. Tectonophysics 491, 211–217.

Royden, L.H., Burchfiel, B.C., King, R.W., Wang, E., Chen, Z., Shen, F., Liu, Y., 1997. Surface deformation and lower crustal flow in eastern Tibet. Science 276 (5313), 788.

Sengör, A.M.C., 1984. The Cimmeride orogenic system and the tectonics of Eurasia. Spec. Pap., Geol. Soc. Am. 195, 1–82.

Shen, Z., Lü, J., Wang, M., Bürgmann, R., 2005. Contemporary crustal deformation around the southeast borderland of the Tibetan Plateau. J. Geophys. Res. 110, B11409. https://doi.org/10.1029/2004JB003421.

Tapponnier, P., Xu, Z., Roger, F., Meyer, B., Arnaud, N., Wittlinger, G., Yang, J., 2001. Oblique stepwise rise and growth of the Tibet plateau. Science 294, 1671–1677.

Tian, X., Zhang, Z., 2013. Bulk crustal properties in NE Tibet and their implications for deformation model. Gondwana Res. 24, 548–559.

Vergne, J., Wittlinger, G., Qiang, H., Tapponnier, P., Poupinet, G., Jiang, M., Herquel, G., Paul, A., 2002. Seismic evidence for stepwise thickening of the crust across the NE Tibetan plateau. Earth Planet. Sci. Lett. 203, 25–33.

Wang, C.S., Gao, R., Yin, A., Wang, H.Y., 2011. A mid-crustal strain-transfer model for continental deformation: a new perspective from high-resolution deep seismic reflection profiling across NE Tibet. Earth Planet. Sci. Lett. 306, 279–288.

Wang, E., Kirby, E., Furlong, K.P., Soest, M.V., Xu, G., Shi, X., Kamp, P., Hodges, K., 2012. Two-phase growth of high topography in eastern Tibet during the Cenozoic. Nat. Geosci. 5 (9), 640–645.

Wang, X., Li, Y., Ding, Z., Zhu, L., Wang, C., Bao, X., Wu, Y., 2017. Three dimensional lithospheric S wave velocity model of the NE Tibetan Plateau and western North China Craton. J. Geophys. Res., Solid Earth 122, 6703–6720. https://doi.org/10.1002/2017JB014203.

Wang, Z., Huang, R.Q., Pei, S.P., 2014. Crustal deformation along the Longmen-Shan fault zone and its implications for seismogenesis. Tectonophysics 610, 128–137.

Watanabe, T., 1993. Effects of water and melt on seismic velocities and their application to characterization of seismic reflectors. Geophys. Res. Lett. 20, 2933–2936. https://doi.org/10.1029/93GL03170.

Wei, Z.G., Chen, L., Li, Z.W., Ling, Y., Li, J., 2016. Regional variation in moho depth and Poisson's ratio beneath eastern china and its tectonic implications. J. Asian Earth Sci. 115, 308–320.

Wu, Q.J., Zeng, R.S., 1998. The crustal structure of Qinghai–Xizang plateau inferred from broadband teleseismic waveform. Chin. J. Geophys. 41, 669–679 (in Chinese).

Wu, Z.B., Xu, T., Badal, J., Yao, H., Wu, C., Teng, J., 2017. Crustal shear-wave velocity structure of northeastern Tibet revealed by ambient seismic noise and receiver functions. Gondwana Res. 41, 400–410.

Wu, Z.B., Xu, T., Liang, C.T., Wu, C.L., Liu, Z.Q., 2018. Crustal shear wave velocity structure in the northeastern Tibet based on the Neighbourhood algorithm inversion of receiver functions. Geophys. J. Int. 212, 1920–1931. https://doi.org/10.1093/gji/ggx521.

Xu, T., Wu, Z., Zhang, Z., Tian, X., Deng, Y., Wu, C., Teng, J., 2014. Crustal structure across the Kunlun fault from passive source seismic profiling in East Tibet. Tectonophysics 627, 98–107.

Yang, J.S., Robinson, P.T., Jing, C.F., Xu, Z.Q., 1996. Ophiolites of the Kunlun Mountains, China and their tectonic implications. Tectonophysics 258, 215–231.

Yin, A., Harrison, T.M., 2000. Geologic evolution of the Himalayan–Tibetan orogen. Annu. Rev. Earth Planet. Sci. 28, 211–280.

Yin, A., 2010. A special issue on the great 12 May 2008 Wenchuan earthquake (Mw 7.9): observations and unanswered questions. Tectonophysics 491, 1–9.

Zhang, Z., Wang, Y., Chen, Y., Houseman, G.A., Tian, X., Wang, E., Teng, J., 2009. Crustal structure across Longmenshan fault belt from passive source seismic profiling. Geophys. Res. Lett. 36, L17310. https://doi.org/10.1029/2009GL039580.

Zhang, Z., Yuan, X., Chen, Y., Tian, X., Kind, R., Li, X.Q., Teng, J., 2010. Seismic signature of the collision between the east Tibetan escape flow and the Sichuan basin. Earth Planet. Sci. Lett. 292 (3–4), 254–264.

Zhang, Z., Klemperer, S., Bai, Z., Chen, Y., Teng, J., 2011. Crustal structure of the Paleozoic Kunlun orogeny from an active-source seismic profile between Moba and Guide in East Tibet, China. Gondwana Res. 19 (4), 994–1007.

Zhao, G.Z., Unsworth, M.J., Zhan, Y., Wang, L.F., Chen, X.B., Jones, A.G., Tang, J., Xiao, Q.B., Wang, J.J., Cai, J.T., Li, T., Wang, Y.Z., Zhang, J.H., 2012. Crustal structure and rheology of the Longmenshan and Wenchuan Mw 7.9 earthquake epicentral area from magnetotelluric data. Geology 40, 1139–1142.

Zheng, T.Y., Chen, L., Zhao, L., Xu, W.W., Zhu, R.X., 2006. Crust–mantle structure difference across the gravity gradient zone in North China Craton: seismic image of the thinned continental crust. Phys. Earth Planet. Inter. 159, 43–58.

Zhu, L., Kanamori, H., 2000. Moho depth variation in southern California from teleseismic receiver functions. J. Geophys. Res. 105, 2969–2980. https://doi.org/10.1029/1999JB900322.